Estimation of High-Resolution Land Surface Shortwave Albedo From AVIRIS Data

Tao He, Shunlin Liang, *Fellow*, *IEEE*, Dongdong Wang, Qinqing Shi, and Xin Tao

***Abstract*—Hyperspectral remote sensing data offer unique opportunities for the characterization of the land surface and atmosphere in the spectral domain. However, few studies have been conducted to estimate albedo from such hyperspectral data. In this study, we propose a novel approach to estimate surface shortwave albedo from data provided by the Airborne Visible Infrared Imaging Spectrometer (AVIRIS). Our proposed method is based on the empirical relationship between apparent directional reflectance and surface shortwave broadband albedo established by extensive radiative transfer simulations. We considered the use of two algorithms to reduce data redundancy in the establishment of the empirical relationship including stepwise regression and principle component analysis (PCA). Results showed that these two algorithms were able to produce albedos with similar accuracies. Analysis was carried out to evaluate the effects of surface anisotropy on the direct estimation of broadband albedo. We found that the Lambertian assumption we made in this study did not lead to significant errors in the estimation of broadband albedo from simulated AVIRIS data over snow-free surfaces. Cloud detection was carried out on the AVIRIS images using a Gaussian distribution matching method. Preliminary evaluation of the proposed method was made using AmeriFlux ground measurements and Landsat data, showing that our albedo estimation can satisfy the accuracy requirements for climate and agricultural studies, with respective root-mean-square-errors (RMSEs) of 0.027, when compared with AmeriFlux, and 0.032, when compared with Landsat. Further efforts will focus on the extension and refinement of our algorithm for application to satellite hyperspectral data.**

***Index Terms*—Airborne Visible Infrared Imaging Spectrometer (AVIRIS), AmeriFlux, bidirectional reflectance distribution function (BRDF), direct estimation, hyperspectral data, Landsat, principle component analysis (PCA), stepwise regression, surface albedo.**

I. Introduction

SURFACE albedo is an important parameter for calculating the surface energy balance, as used in urban environment studies [1], [2]. High-resolution albedo maps can also be used as a critical input for the estimation of the surface energy budget, to improve the estimation of evapotranspiration in precision agriculture studies [3]. Supply of albedo values at high spatial resolutions also enables ecological studies of the surface energy balance at landscape scales, where surface albedo is sensitive to small-scale vegetation structure [4].

Manuscript received September 23, 2013; revised January 15, 2014; accepted January 20, 2014. Date of publication February 05, 2014; date of current version January 21, 2015. This work was supported by the NASA HyspIRI preparatory Grant NNH11ZDA001N-HYSPIRI from the University of Maryland, College Park, MD, USA.

The authors are with the Department of Geographical Sciences, University of Maryland, College Park, MD 20742 USA (e-mail: the@umd.edu).

Color versions of one or more of the figures in this paper are available online at http://ieeexplore.ieee.org.

Digital Object Identifier 10.1109/JSTARS.2014.2302234

Global land surface albedo products have been generated from multiple satellite sensors [5]. In general, there are two approaches estimating land surface albedo [6], [7]: physical and statistical. The physical approach, adopted by the Moderate Resolution Imaging Spectroradiometer (MODIS) land team [8], generally consists of three basic steps: 1) atmospheric correction that converts top-of-atmosphere (TOA) radiance to surface directional reflectance; 2) surface anisotropic model fitting that converts accumulated surface directional reflectance to spectral albedos [9]; and 3) narrowband to broadband conversion that converts spectral albedo to broadband albedo. An optimization-based method has also been developed to simultaneously retrieve surface albedo and aerosol optical depth, based on the coupling of atmosphere and surface anisotropy in radiative transfer models [10].

In comparison, the statistical approach directly links TOA spectral reflectance to land surface broadband albedo, based on a database created from extensive radiative transfer simulations. The statistical method does not require any atmospheric correction. Moreover, it also does not require the accumulation of observations over a certain period of time, which enables the monitoring of rapid changes in surface albedo. Liang *et al.* [11] designed a direct estimation algorithm using a neural-network. This was later improved using linear regression analysis for each of the angular bins and applied to MODIS data [12] and was also improved to produce accurate daily snow/ice albedo more efficiently with a mean bias of less than 0.02 and residual standard error of 0.04 [13]. This algorithm has been adopted as a default for operationally mapping the land surface broadband albedo using data from the Visible Infrared Imager Radiometer Suite (VIIRS), and it has recently been improved by Wang *et al.* [14]. In addition, the algorithm has also been further refined to produce the long-term Global LAnd Surface Satellites (GLASSs) albedo product [15], [16].

In the past decade, few researchers have used hyperspectral remote sensing data to estimate surface broadband albedo, either due to its limited temporal and spatial coverage, or to the challenge posed by the automation of pixel-level atmospheric correction. For example, Painter *et al.* [17] established the relationship between surface albedo and snow cover as well as snow grain size, based on model-simulated spectral libraries. They then applied this relationship to atmospherically corrected surface reflectance to estimate albedo. Roberts *et al.* [4] used modeled surface downward radiation and atmospherically corrected surface reflectance to calculate shortwave albedo. Both the studies followed the above-mentioned physical approach to estimate albedo. However, in these approaches, the atmospheric components must be premeasured to obtain the surface reflectance, under the Lambertian assumption.

The nature of the direct albedo estimation algorithm is such that it relies on the data from extensive radiative transfer simulations under different geometries and atmospheric conditions, to overcome the lack of premeasured atmospheric components needed for atmospheric correction. As the direct estimation algorithm is based heavily on spectral signatures, hyperspectral data would be more useful than multispectral data to examine its performance in albedo estimation, without using angular signatures. In this study, we developed a refined direct estimation algorithm and used it on the Airborne Visible Infrared Imaging Spectrometer (AVIRIS) data, as a proxy for hyperspectral satellite data, to ultimately estimate surface shortwave albedo. In this paper, we first introduce the AVIRIS data and basic principles of directly estimating surface albedo from hyperspectral data in Section II. Preliminary results and validations are shown and discussed in Section III, followed by the conclusion in Section IV.

II. Methodology and Data

A. Direct Estimation of Surface Albedo From Hyperspectral Data

Surface shortwave albedo, defined as the ratio of outgoing to incoming solar radiation at the Earth's surface, is a very important biophysical variable in climate, urban, agricultural, and ecological studies. Surface shortwave albedo can be calculated as the sum of spectral albedo, weighted by the downward solar radiation [7]

$$\alpha_{sw} = \int_{\lambda_1}^{\lambda_2} \alpha_\lambda F_\lambda^d d\lambda \Big/ \int_{\lambda_1}^{\lambda_2} F_\lambda^d d\lambda \tag{1}$$

where α_{sw} is the surface shortwave albedo covering the spectral range from λ_1 (300 nm) to λ_2 (3000 nm); F_λ^d and α_λ are the surface downward shortwave radiation and spectral albedo at wavelength λ, respectively.

Surface spectral albedo α_λ is the integrated value of the atmospherically corrected surface directional reflectances over the entire hemisphere. For multispectral sensors, shortwave albedo is usually calculated from the spectral albedos of multiple bands [8], [18]. While surface spectral reflectance can usually be derived from atmospheric correction of a single observation (apparent reflectance or radiance), spectral albedo requires multiple angular samplings for integration over the hemisphere, which is usually not possible with sensors such as AVIRIS. Although surface shortwave albedo needs both spectral and angular information, the latter is currently not available for hyperspectral behavior. However, previous studies have shown that the Lambertian assumption for hyperspectral data in broadband albedo estimations does not lead to significant errors [13], [19]. In other words, the abundant spectral information from hyperspectral data can compensate for the errors inherent in the Lambertian assumption we applied to the albedo estimation in this study.

Traditional methods of atmospheric correction require atmospheric variables such as aerosol loading and water vapor content as inputs. Errors in the atmospheric variable estimation will propagate into the final surface albedo estimation. Moreover, the TOA solar radiation is usually used as a weighting factor in (1) to calculate shortwave albedo. However, the solar radiation that reaches the Earth's surface at a specific time, elevation, and geographic location will be redistributed in the spectral domain by means of absorption and scattering of the atmosphere. Thus, the actual surface shortwave albedo will change with the atmospheric conditions, including aerosol loading and other factors.

Hyperspectral data are capable of capturing the spectral signatures of both the surface and atmosphere, providing an accurate broadband surface albedo estimation [19]. To overcome the above-mentioned limitations, the following direct estimation designed by Liang *et al.* [13] could be refined to retrieve surface albedo from a single observation

$$\alpha_{sw} = \sum_{i=1}^{n} a_i \rho_i + a_0 \tag{2}$$

where ρ_i is the apparent reflectance observed by the remote sensor for band $i \in [1, n]$; a_i is the regression coefficient; and a_0 is the intercept.

Fig. 1 illustrates the procedure for estimating surface shortwave albedo from hyperspectral remote sensing data. To carry out the direct estimation, we first collected 245 surface albedo spectra including vegetation, soil, rock, water, snow, and ice [6], [10] from USGS [20] and ASTER [21] libraries and used MODTRAN5 [22] to simulate the shortwave albedo and the apparent reflectance for each spectral band under different geometric and atmospheric conditions (see Table I). We used the "US62" atmospheric profile. Precipitable water vapor was set at 1.5 cm based on previous research [1]. "Rural aerosol" was taken as the primary aerosol type in the simulations [22].

Given that many spectral bands are inter-correlated, application of the direct estimation using all the bands would not be necessary and may even cause problems of over-fitting. Water vapor absorption bands and low signal-to-noise-ratio (SNR) bands were removed for this estimation of surface albedo.

The magnitude of the apparent reflectance changes with sun-sensor-target geometries and atmospheric conditions. We therefore carried out the linear regression for each of the angular bins (Table I) to improve the accuracy of the estimation. As much of the information from hyperspectral data is inter-correlated, it is important to remove the redundant bands in order to further mitigate the over-fitting problem. Thus, in this study, we propose the use of two algorithms: stepwise regression and principle component analysis (PCA). For the stepwise regression method, we used a backward stepwise regression algorithm. In the variable selection of the stepwise regression, bands with p values less than 0.05 were removed. For the PCA-based method, we first carried out the PCA for each of the angular bins. Then, we selected the principle components that explained 99% of sample variance. Finally, regressions between the apparent reflectance and principle components were carried out. Some results, based on the radiative transfer simulations, are presented in Section III-A.

B. AVIRIS Data

AVIRIS is an airborne sensor that is operated by the NASA Jet Propulsion Laboratory (JPL) and flies onboard ER-2 and Twin Otter aircrafts mainly over the United States. The AVIRIS

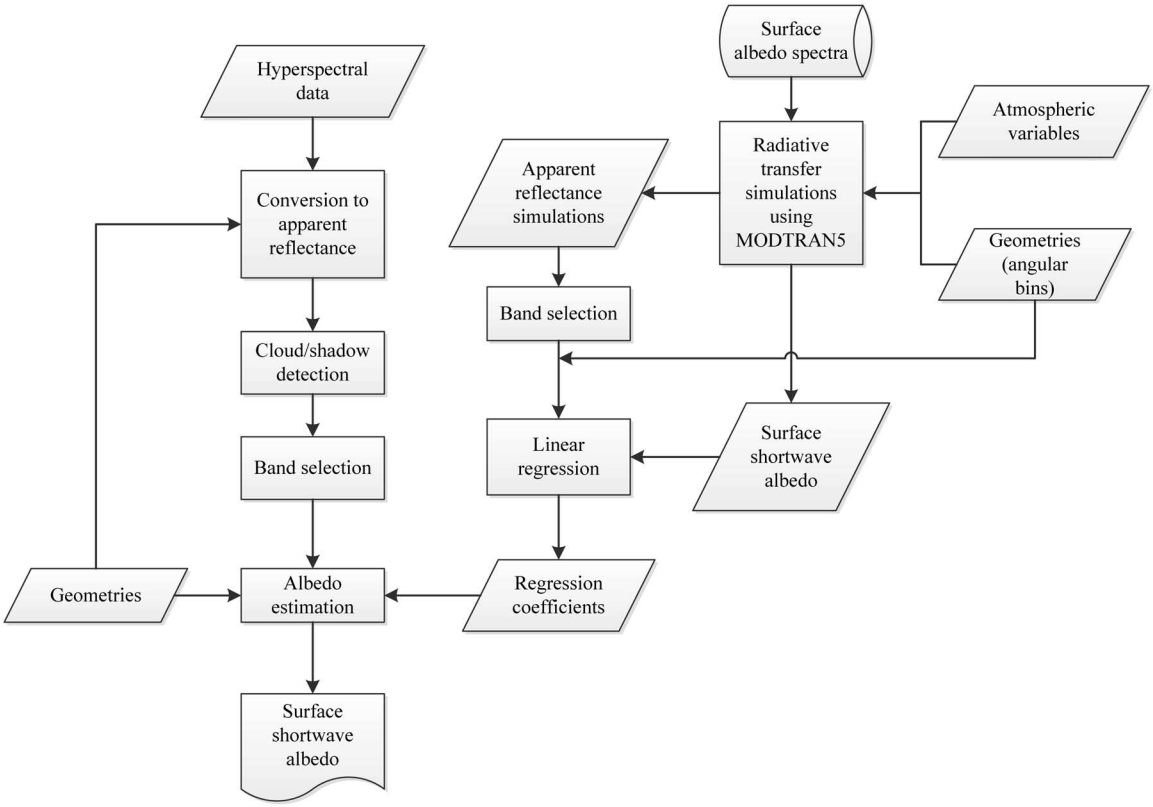

Fig. 1. Flowchart of surface albedo estimation from hyperspectral remote sensing data.

TABLE I
CONFIGURATION OF GEOMETRIC AND ATMOSPHERIC CONDITIONS IN MODTRAN5 SIMULATIONS

Parameter	Values
View zenith angle (°)	0, 5, 10,15, and 20
Solar zenith angle (°)	20, 25, 30, 35, 40, and 45
Relative azimuth angle (°)	0, 30, 60, 90, 120, 150, and 180
Visibility (km)	2, 3, 4, 5, 10, 15, 20, 25, 30, 50, and 100

sensor consists of 224 spectral bands in the range of 300–2500 nm, with an average bandwidth of 10 nm. It has an off-nadir scan angle of $\pm 14^{\circ}$ and its spatial resolution varies from ~ 3 to ~ 17 m depending on the flight altitude from 4 to 20 km. AVIRIS data after 2006 are freely available through the JPL website. All the data have been geometrically and radiometrically calibrated [23].

C. AmeriFlux Ground Measurements

Ground measurements of downward and upward shortwave radiation are available from AmeriFlux sites over the North America. Measurements are routinely made and recorded at intervals of 30 min with a spectral coverage of 250–2800 nm. Surface albedo can be calculated by dividing the upward radiation by the downward radiation. We compiled and utilized all the available AVIRIS data and AmeriFlux measurements for 2007–2011. Matches were tabulated in Table II.

III. RESULTS

A. Empirical Relationship of Surface Albedo and Apparent Reflectance From Radiative Transfer Simulations

Following the methodology introduced in Section II, we used MODTRAN5 [22] and the surface spectra to simulate the broadband surface albedo and apparent spectral reflectance under different geometric and atmospheric conditions.

A least-square linear regression algorithm was applied to establish the relationship between surface albedo and apparent reflectance from the simulated data, following (2). Regression for each angular bin was carried out separately. Tables III and IV show examples (view zenith angle $= 5^{\circ}$) of the root-mean-square-error (RMSE) and R^2 from the stepwise regression algorithm and PCA-based algorithm, respectively.

In the stepwise regression algorithm, generally, fewer than 10 bands are selected for each of the angular bins after application of the band removal criteria. All the R^2 values are greater than 0.99, which indicates good performance of the linear regression among different land cover types under different atmospheric conditions. RMSE values are less than 0.01 when the solar zenith angle is small ($<35^{\circ}$). As the solar zenith angle reaches 40°, the RMSE values become slightly larger than 0.01, which is still very good. This suggests that a larger solar zenith angle introduces larger uncertainties in the surface albedo estimation, which is likely caused by the increased length of path through the atmosphere. The results from the PCA-based algorithm are slightly inferior to those from the stepwise regression algorithm; the RMSE is almost doubled while the R^2 is slightly smaller but still larger than 0.98.

TABLE II
AVIRIS FLIGHTS OVER AMERIFLUX SITES DURING 2007–2011 WITH VALID GROUND SHORTWAVE ALBEDO MEASUREMENTS

Site	Lat/Lon[a]	IGBP[b]	Flight no.	Year	DOY[c]	UTC	Pixel size	SZA[d]
US-Var	38.407, –120.951	GRA	f070805t01p00r05	2007	217	18:59	3.2	26.5
			f070805t01p00r07	2007	217	19:25	3.2	23.7
US-NR1	40.033, –105.546	ENF	f100825t01p00r07	2010	237	18:11	13.9	31.6
			f110807t01p00r06	2011	219	16:42	8.9	39.4
			f110807t01p00r10	2011	219	17:30	9.3	31.8
			f110807t01p00r18	2011	219	18:53	9	23.9
US-Skr	25.365, –81.078	EBF	f100523t01p00r12	2010	143	15:30	17	26.0
US-UMB	45.560, –84.714	DBF	f090704t01p00r10	2009	185	17:28	16.9	22.9
			f110814t01p00r12	2011	226	18:17	16.8	32.0
			f110816t01p00r13	2011	228	17:05	16.7	32.9
US-Ne1	41.165, –96.477	CRO	f080713t01p00r09	2008	195	17:16	16.9	25.2
			f080713t01p00r10	2008	195	17:27	16.9	23.7
US-Ne3	41.180, –96.440	CRO	f080713t01p00r09	2008	195	17:16	16.9	25.2
			f080713t01p00r10	2008	195	17:27	16.9	23.7
US-ChR	35.931, –84.332	DBF	f090724t01p00r06	2009	205	15:19	4.6	35.5
US-Los	46.083, –89.979	CSH	f080709t01p00r10	2008	191	17:09	16.8	26.4
			f080714t01p00r06	2008	196	17:03	16.8	27.7
US-CaV	39.063, –79.421	GRA	f090706t01p00r12	2009	187	16:06	15.9	23.0
US-UMd	45.563, –84.698	DBF	f090704t01p00r10	2009	185	17:28	16.9	22.9
			f110814t01p00r12	2011	226	18:17	16.8	32.0
			f110816t01p00r13	2011	228	17:05	16.7	32.9

[a]Precise geo-location information can be found in AmeriFlux website.
[b]IGBP: International Geosphere-Biosphere Programme; CRO: cropland; CSH: closed shrubland; DBF: deciduous broadleaf forest; EBF: evergreen broadleaf forest; ENF: evergreen need leaf forest; GRA: grassland.
[c]DOY: day of year.
[d]SZA: solar zenith angle.

TABLE III
STATISTICS USING STEPWISE REGRESSION TO ESTIMATE SURFACE SHORTWAVE ALBEDO FROM SIMULATED DATA (VIEW ZENITH ANGLE: 5°): (A) RMSE; (B) R^2

		(a) Relative azimuth angle						
		0°	30°	60°	90°	120°	150°	180°
Solar zenith angle	20°	0.0082	0.0082	0.0082	0.0082	0.0082	0.0082	0.0082
	25°	0.0085	0.0086	0.0086	0.0085	0.0086	0.0085	0.0085
	30°	0.0088	0.0087	0.0087	0.0087	0.0087	0.0087	0.0089
	35°	0.0099	0.0101	0.0101	0.0093	0.0091	0.0092	0.0091
	40°	0.0110	0.0111	0.0109	0.0113	0.0111	0.0105	0.0106
	45°	0.0115	0.0114	0.0114	0.0113	0.0112	0.0111	0.0112

		(b) Relative azimuth angle						
		0°	30°	60°	90°	120°	150°	180°
Solar zenith angle	20°	0.9965	0.9965	0.9965	0.9965	0.9965	0.9965	0.9965
	25°	0.9962	0.9962	0.9961	0.9962	0.9961	0.9962	0.9962
	30°	0.9960	0.9960	0.9961	0.9960	0.9961	0.9961	0.9959
	35°	0.9949	0.9947	0.9947	0.9955	0.9957	0.9956	0.9957
	40°	0.9937	0.9936	0.9938	0.9933	0.9936	0.9943	0.9942
	45°	0.9931	0.9932	0.9933	0.9934	0.9935	0.9936	0.9935

TABLE IV
STATISTICS USING PRINCIPLE COMPONENTS TO ESTIMATE SURFACE SHORTWAVE ALBEDO FROM SIMULATED DATA (VIEW ZENITH ANGLE: 5°): (A) RMSE; (B) R^2

		(a) Relative azimuth angle						
		0°	30°	60°	90°	120°	150°	180°
Solar zenith angle	20°	0.0153	0.0153	0.0153	0.0154	0.0154	0.0154	0.0154
	25°	0.0158	0.0158	0.0158	0.0159	0.0159	0.0159	0.0159
	30°	0.0164	0.0164	0.0164	0.0164	0.0164	0.0164	0.0164
	35°	0.0171	0.0171	0.0171	0.0171	0.0170	0.0170	0.0169
	40°	0.0179	0.0179	0.0179	0.0178	0.0178	0.0177	0.0177
	45°	0.0189	0.0189	0.0188	0.0187	0.0185	0.0184	0.0184

		(b) Relative azimuth angle						
		0°	30°	60°	90°	120°	150°	180°
Solar zenith angle	20°	0.9879	0.9879	0.9879	0.9878	0.9878	0.9877	0.9877
	25°	0.9872	0.9871	0.9871	0.9870	0.9870	0.9870	0.9870
	30°	0.9861	0.9861	0.9861	0.9861	0.9861	0.9861	0.9861
	35°	0.9848	0.9848	0.9849	0.9849	0.9850	0.9851	0.9851
	40°	0.9833	0.9833	0.9834	0.9835	0.9836	0.9838	0.9838
	45°	0.9814	0.9814	0.9816	0.9818	0.9821	0.9823	0.9824

B. Surface Anisotropic Effects in the Broadband Albedo Direct Estimation

To simplify the procedure for albedo estimation using hyperspectral data in this study, the Lambertian assumption was adopted. The findings of [13], [19] indicated that this assumption would not lead to significant bias in the broadband albedo estimation that uses hyperspectral information. Nevertheless, it is important to investigate the surface anisotropic effects in our direct estimation of broadband albedo from AVIRIS data.

In this study, we simulated snow-free surface bidirectional reflectance distribution functions (BRDFs) using the Scattering by Arbitrarily Inclined Leaves (SAIL) model [24], [25] under various illumination geometries, vegetation densities, and structures (see Table V). Soil spectra from the spectral libraries (see Section II-A) were also used in the surface BRDF simulations. Based on the surface BRDFs, we then simulated the AVIRIS TOA spectral reflectance using the same geometric and atmospheric configurations as listed in Table I, except that we extended the range of view zenith angle $0°$–$75°$.

The regression coefficients derived from the stepwise regression algorithm in Section II-A were directly applied to the simulated

TABLE V
CONFIGURATION OF GEOMETRIC AND VEGETATION CONDITIONS IN SURFACE BRDF SIMULATIONS

Parameter	Values
Leaf area index	0.01, 0.10, 0.25, 0.50, 0.75, 1.00, 1.50, 2.00, 3.00, and 7.00
Leaf angle distribution type	Erectophile, plagiophile, planophile, spherical, and uniform
View zenith angle (°)	0, 15, 30, 45, 60, and 75

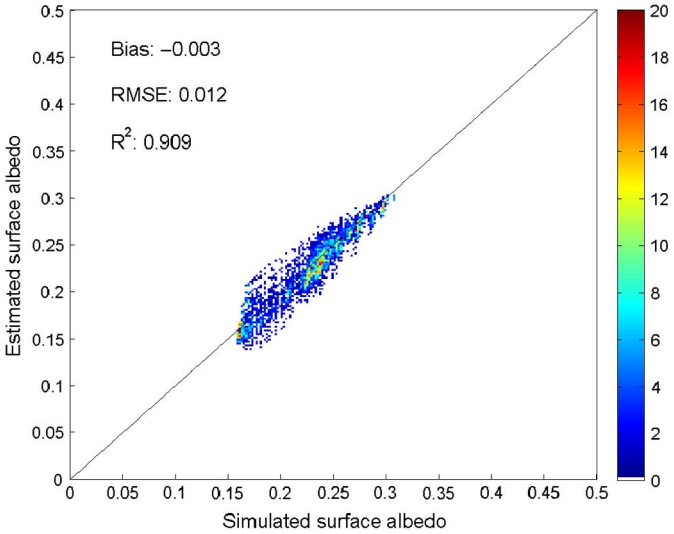

Fig. 2. Comparison of albedo estimation from simulated AVIRIS TOA reflectance (y-axis) and surface albedo integrated from SAIL model simulated surface BRDF (x-axis). Color bar shows point density.

TABLE VI
ALBEDO ESTIMATION ACCURACY AND VIEW ZENITH ANGLE (SOLAR ZENITH ANGLE: 35°)

Variable	Value				
View zenith angle (°)	0	15	30	45	60
RMSE	0.0155	0.0100	0.0091	0.0104	0.0147
R^2	0.9181	0.9505	0.9493	0.9261	0.8596

AVIRIS TOA reflectance to generate the surface albedo estimation. Comparison between the estimated albedo and the SAIL simulated surface albedo (Fig. 2) shows that our albedo estimates have a small negative bias (-0.003) with an RMSE of 0.012. This supports the assertion that the Lambertian assumption does not lead to significant errors in the surface broadband albedo estimation from hyperspectral data, particularly for snow-free surfaces.

Table VI shows the impacts of the view zenith angle on the albedo estimation. The results indicate that the albedo estimation accuracies do not change much with different view zenith angles. Considering that both the solar zenith angle and the view zenith angle from AVIRIS data selected in this study are within the range of $0°$–$45°$, direct application of the linear relationship between TOA reflectance and surface broadband albedo derived in this study would be able to satisfy the accuracy requirements.

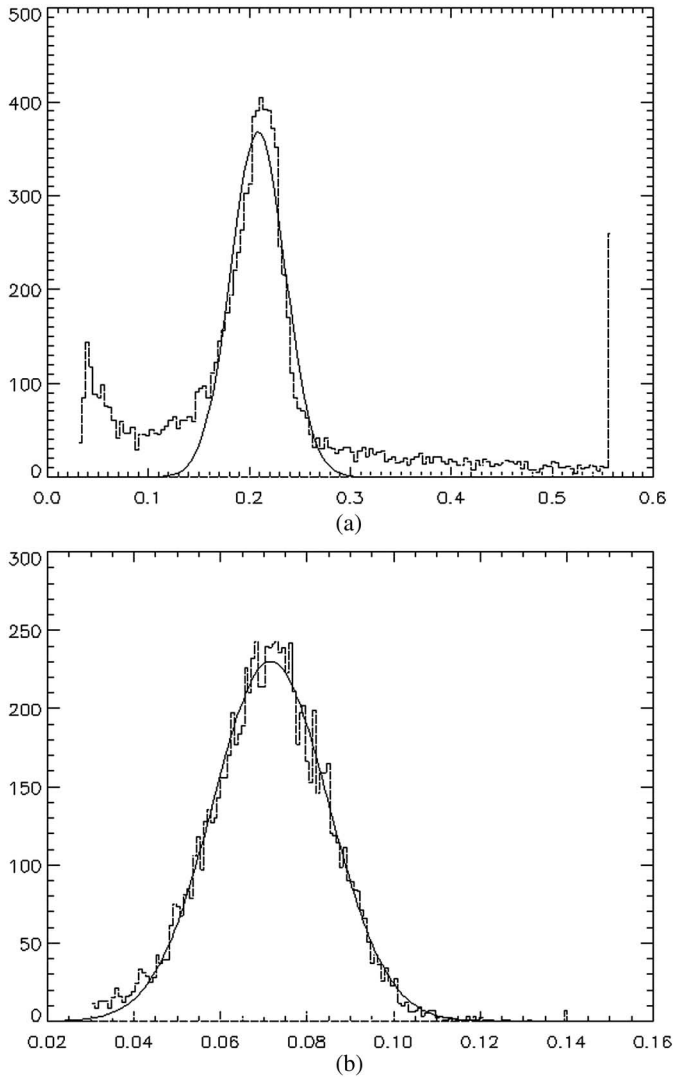

Fig. 3. Gaussian distribution curve fitted to the histogram of apparent radiance for cloud detection using AVIRIS band 1.38 μm: (a) cloudy image at site US-CaV on DOY 187, 2009 and (b) cloud-free image at site US-ChR on DOY 205, 2009.

C. Cloud Detection From AVIRIS Data

Detection of cloud cover from AVIRIS data is difficult without the simultaneous thermal infrared observations. The spectral signatures of cloud and land surface would be highly variable as the solar-sensor-target geometries change. Simply relying on the spectral threshold approach may result in significant uncertainties in cloud detection. Therefore, spatial information is required for cloud detection if the scene is not entirely covered by clouds.

In this study, before we carry out any cloud detection, we have to make the assumption that the surface albedo of a snow-free area follows a Gaussian distribution. We selected the apparent reflectance data of AVIRIS band 1.38 μm [26], [27] and fit its histogram with a Gaussian distribution. Data that fell outside 2σ of the Gaussian distribution were assumed to be either clouds (high reflectance) or shadows (low reflectance). We tested the cloud detection algorithm and found that it worked well on all the data listed in Table II based on visual interpretation. Examples of cloud detection in cloudy and clear scenes are shown in Figs. 3 and 4.

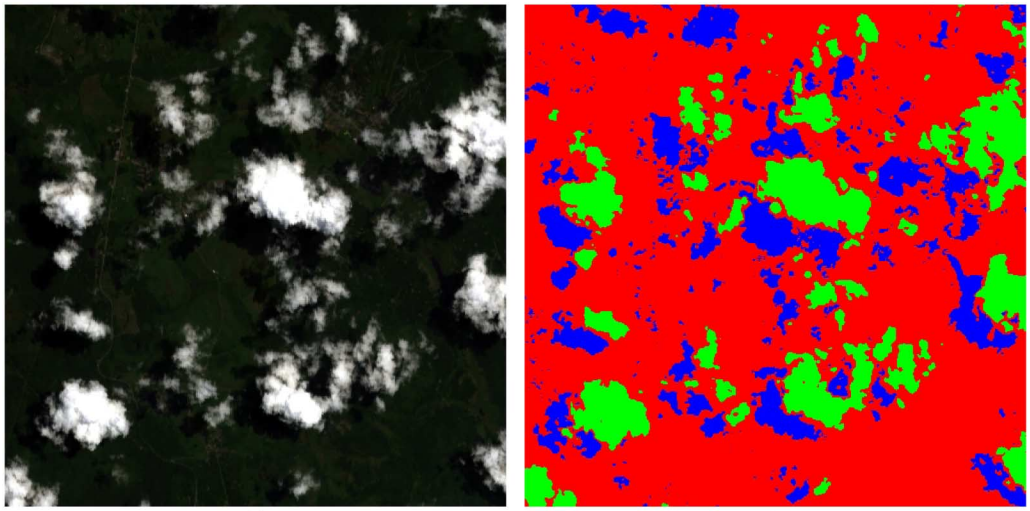

Fig. 4. Detection of cloud/shadow from AVIRIS data: (a) true color composite of AVIRIS data at site US-CaV on DOY 187, 2009 and (b) detection results from the AVIRIS data (land: red, cloud: green, and shadow: blue).

One limitation of cloud/shadow detection in AVIRIS data is that shadows and water bodies are indistinguishable from one another because of their similar signature in the shortwave spectral domain. Further improvement to cloud/shadow detection may involve the geometric linkage between cloud and shadow to reduce potential misclassification of shadow and water.

D. Estimation of Surface Albedo at AmeriFlux Sites

Direct comparison of remotely sensed albedo with ground measurements is not usually optimal since: 1) remote sensing sensors obtain information on a pixel-basis instead of a point-basis and 2) the footprint of the pyranometer is determined by its height and field-of-view (FOV). The high spatial resolution of AVIRIS data offers unique opportunities for accurate matching of ground measurements with remote sensing data compared to coarse-resolution data. We followed the methodology presented in He *et al.* [6] and Shuai *et al.* [28] using the instrument height and FOV to calculate the effective footprint of ground measurements. Then, we aggregated the corresponding AVIRIS pixels to obtain the AVIRIS albedo for each site. Ground measurements were averaged using data obtained within ± 30 min of the flight overpass to match the AVIRIS data. In this way, we could minimize the difference in scale between remotely sensed albedo and ground measurements.

The comparison of AVIRIS albedo and ground measurements at 10 AmeriFlux sites is shown in Fig. 5. According to Table II, some flights covered multiple AmeriFlux sites and some sites were observed by the flights multiple times. Results show that our algorithms used to estimate AVIRIS albedo are effective over snow-free surfaces, with a bias of -0.003 and an RMSE of 0.027 for the stepwise regression algorithm and a bias of 0.004 and an RMSE of 0.031 for the PCA-based algorithm. This also indicates that our algorithms are robust for flights ~ 20 km above sea level, regardless of flight location. Similar to the simulated results discussed in Section III-A, the results from the PCA-based algorithm are slightly inferior to those from the stepwise regression algorithm. We separated the comparisons shown in

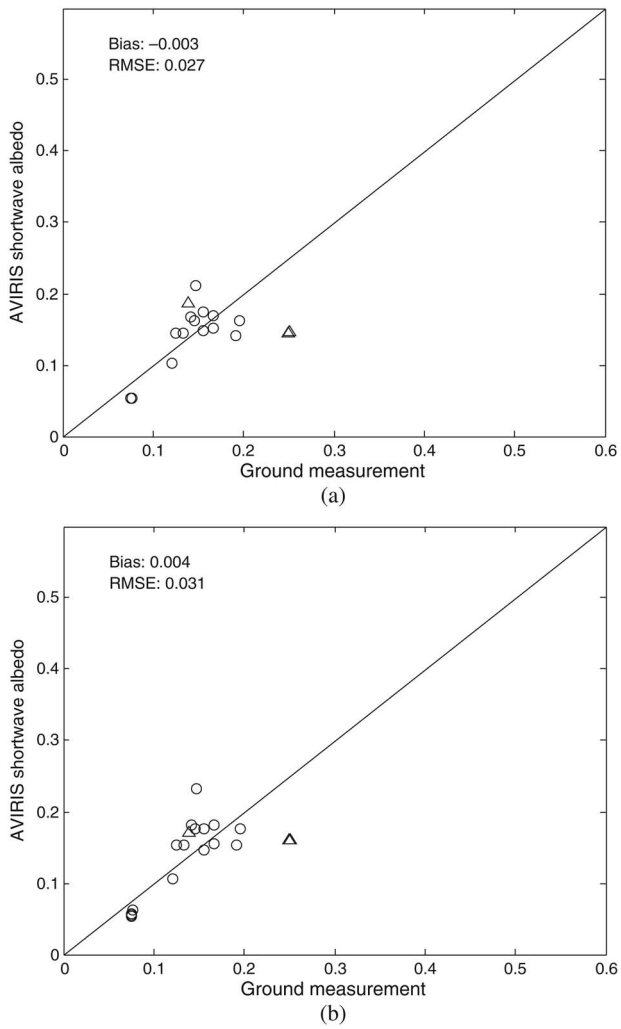

Fig. 5. Comparison of ground measurements and AVIRIS shortwave albedo estimates from (a) the stepwise regression algorithm and (b) the PCA-based algorithm at AmeriFlux sites. Statistics shown in the figure are based on flights with resolutions coarser than 8 m (circles). Flights with finer resolutions (<8 m) are denoted by triangles.

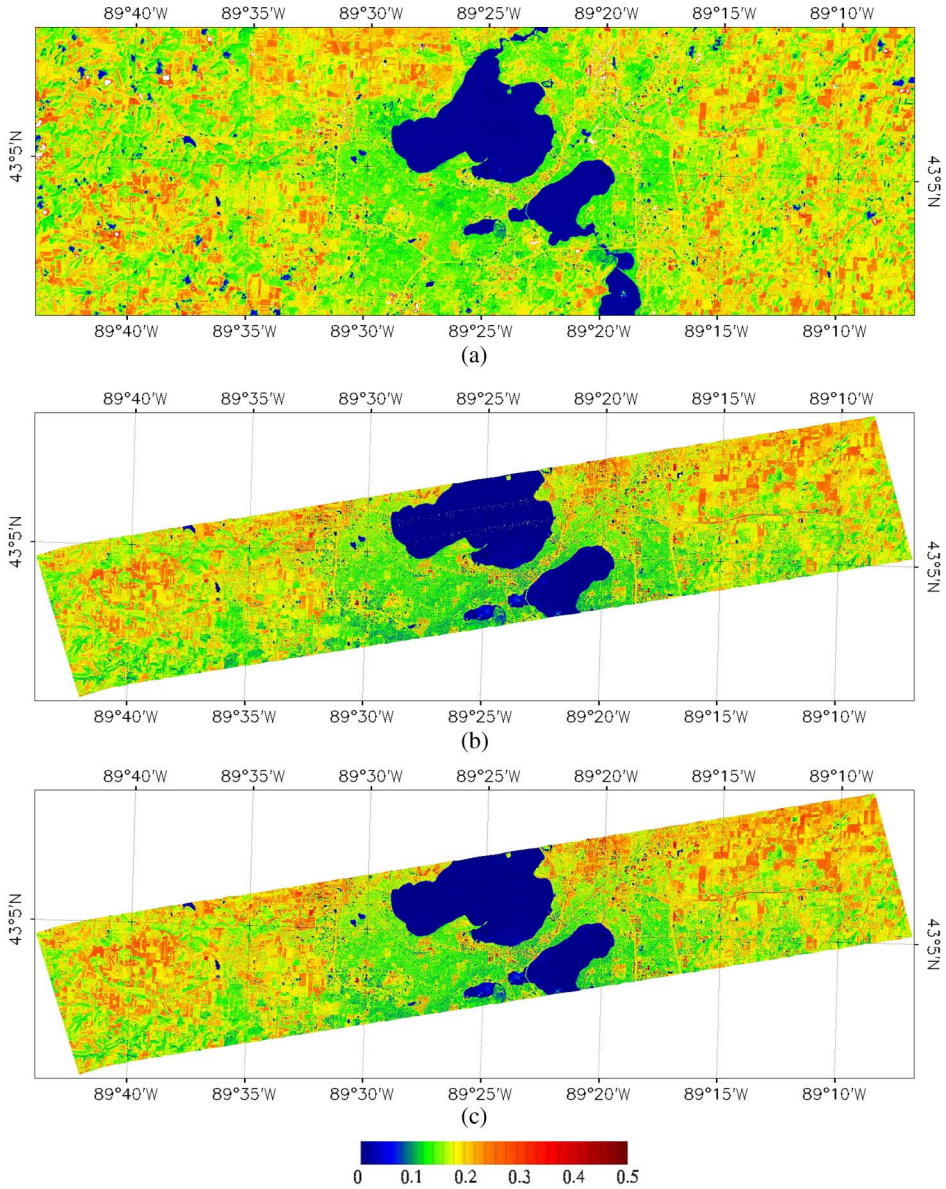

Fig. 6. Shortwave albedo estimations from: (a) Landsat TM on August 18, 2010; (b) AVIRIS on August 26, 2010 using the stepwise regression algorithm; and (c) as for (b) but using the PCA-based algorithm. Image is centered at $43.08°$N, $89.41°$W in Madison, WI, USA.

Fig. 5 by the spatial resolutions of the AVIRIS images. Underestimations of AVIRIS albedo were found at US-Var (the two triangles in Fig. 5) with ground measured albedo of $\sim$0.25 and AVIRIS albedo of $\sim$0.15. US-Var is a grassland site (see Table II) and the instrument was located 2 m above the ground. Thus, a small geolocation error in the high-resolution AVIRIS data (3.2 m at US-Var) would have caused substantial mismatch with the instrument footprint. The surrounding forests may have compounded in this underestimation.

E. Comparison of Albedo Estimations From AVIRIS and Landsat Data

The number of matched pairs of ground measurements made at AmeriFlux sites and AVIRIS flights was limited during 2007–2011. In order to assess our albedo algorithm over a large area covering multiple land cover types, including vegetation, water, bare soil, and urban areas, we used Landsat data to support the validation.

There are three main steps involved in calculating the surface shortwave broadband albedo from Landsat data [6]. First, we used the Landsat Ecosystem Disturbance Adaptive Processing System (LEDAPS) tool to perform the atmospheric correction to obtain surface directional reflectance for each of the six reflective bands and cloud mask [29]. Second, we used MODIS albedo/BRDF products [8] to convert the surface directional reflectance to spectral albedo. Finally, shortwave broadband albedo was calculated from the spectral albedos using an empirical method [6]. This approach of deriving Landsat shortwave albedo has been validated using ground measurements [6], [28].

In the selection of the AVIRIS and Landsat Thematic Mapper (TM) data for algorithm comparison, we considered only the

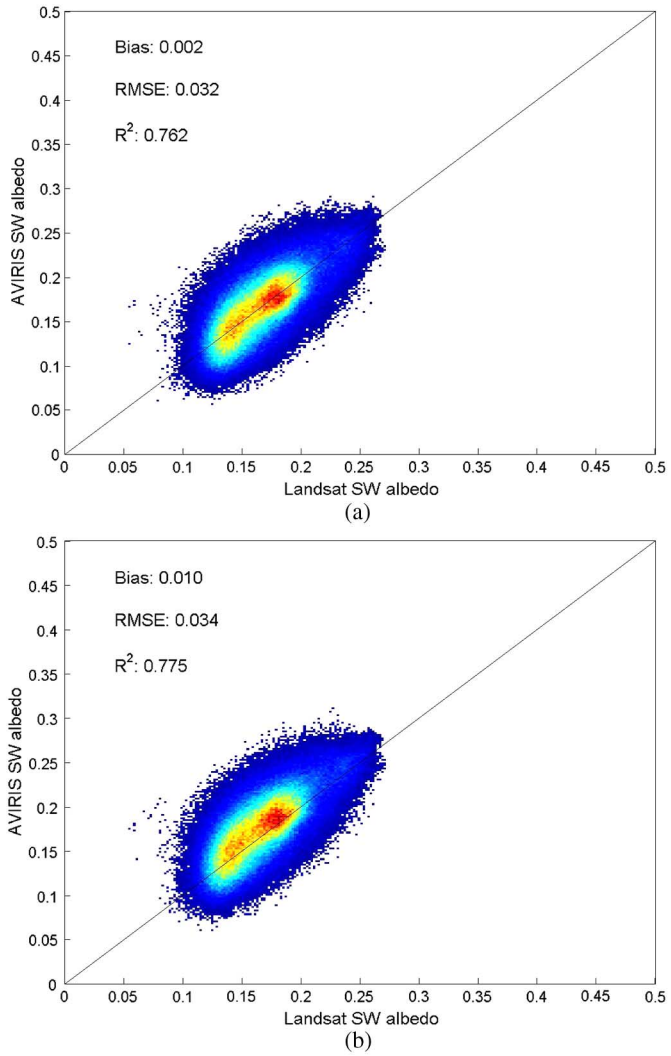

Fig 7. Scatter plots of albedo estimations from Landsat TM and AVIRIS data: (a) AVIRIS albedo estimation from stepwise regression algorithm and (b) AVIRIS albedo estimation from the PCA-based algorithm.

cloud-free scenes with minimal difference in acquisition time. A matched pair of AVIRIS data (flight no.: f100826t01p00r07 on August 18, 2010) and a Landsat TM scene (p024r030 on August 26, 2010) was examined. Considering that both data sets were obtained in August 2010, we assume that there were no significant changes in surface albedo during the 8 days separating their collection. Fig. 6 shows the surface broadband albedo maps from Landsat and AVIRIS. Clear boundaries can be seen in both maps, delineating a variety of land surface types, including water, crop, grass, forest, bare land, and urban areas. A statistical comparison is shown in Fig. 7, which indicates that our algorithm is able to generate promising high-resolution albedo estimates with a bias of 0.002 and an RMSE of 0.032 from the stepwise regression algorithm and a bias of 0.010 and an RMSE of 0.034 from the PCA-based algorithm. The PCA-based algorithm-generated albedo estimations gave an overestimation of 0.008 relative to the stepwise regression algorithm. However, the albedos estimated using the PCA-based algorithm had better overall correlation with the Landsat albedos. In general, no significant differences were found between these two algorithms either from visual comparison (Fig. 6) or from statistical comparison (Fig. 7). These results suggest that our estimated shortwave albedo data are able to satisfy the accuracy requirements of urban, agricultural, ecological, and climate applications.

IV. Conclusion

Estimation of surface shortwave albedo using data of either high spatial resolution or high spectral resolution has seldom been attempted in previous research. In this study, we proposed a refined direct estimation approach using a stepwise regression algorithm and a PCA-based algorithm to estimate shortwave albedo from hyperspectral remote sensing data.

As the Lambertian assumption was made in this study, surface anisotropic effects on the broadband albedo direct estimation have been evaluated. We used the surface BRDFs simulated from a canopy radiation transfer model to estimate surface broadband albedo and to simulate AVIRIS TOA reflectance. Validation results showed that directly applying the Lambertian-based regression coefficients generated accurate surface broadband albedo with an RMSE of 0.012 over snow-free surfaces, and no significant angular dependence. Thus, we argue that hyperspectral information is likely to be more important than the angular information in estimating surface broadband albedo.

The proposed method was applied to AVIRIS data. Preliminary validation results based on ground measurements and Landsat data have shown that our algorithms were robust over various atmospheric and geometric conditions by providing albedo estimation with RMSEs less than 0.034.

Direct comparison with ground measurements has been widely used to assess the medium/coarse resolution satellite albedo products; however, significant differences in scale were found. High spatial resolution albedo estimates can help bridge this gap [30]. In addition, the AVIRIS albedo derived in this study can be very useful in urban environmental, ecological, and agricultural applications, which usually require surface energy balance components with a high spatial resolution.

The principle outcome of this study is that our algorithm can be refined and applied on future satellite hyperspectral missions (e.g., HyspIRI), thereby providing accurate surface albedo estimations on a global basis, as a supplement to the existing satellite products. In addition, the results from our algorithm may be used to verify and explain the possible uncertainties in narrowband to broadband albedo conversions reported in Govaerts *et al.* [31]. Further study is needed, including the implementation of our algorithm to satellite hyperspectral data, and algorithm validation and refinement over bright surfaces, including snow and desert.

Acknowledgments

The authors would thank the AVIRIS team for preprocessing the AVIRIS data; the Ameriflux PIs and staff for providing the ground measurements; and the LEDAPS team members for providing the LEDAPS tool.

References

[1] D. A. Roberts, D. A. Quattrochi, G. C. Hulley, S. J. Hook, and R. O. Green, "Synergies between VSWIR and TIR data for the urban environment: An evaluation of the potential for the Hyperspectral Infrared Imager (HyspIRI) decadal survey mission," *Remote Sens. Environ.*, vol. 117, pp. 83–101, Feb. 2012.

[2] Q. Weng, X. Hu, D. A. Quattrochi, and H. Liu, "Assessing intra-urban surface energy fluxes using remotely sensed ASTER imagery and routine meteorological data: A case study in Indianapolis, U.S.A.," *IEEE J. Sel. Topics Appl. Earth Observ. Remote Sens.,* 2014, doi: 10.1109/JSTARS.2013.2281776.

[3] Z. Su, "The Surface Energy Balance System (SEBS) for estimation of turbulent heat fluxes," *Hydrol. Earth Syst. Sci.*, vol. 6, pp. 85–99, Feb. 2002.

[4] D. A. Roberts, S. L. Ustin, S. Ogunjemiyo, J. Greenberg, S. Z. Dobrowski, J. Q. Chen *et al.*, "Spectral and structural measures of northwest forest vegetation at leaf to landscape scales," *Ecosystems*, vol. 7, pp. 545–562, Aug. 2004.

[5] S. L. Liang, K. C. Wang, X. T. Zhang, and M. Wild, "Review on estimation of land surface radiation and energy budgets from ground measurement, remote sensing and model simulations," *IEEE J. Sel. Topics. Appl. Earth Observ. Remote Sens.*, vol. 3, pp. 225–240, Sep. 2010.

[6] T. He, S. Liang, D. Wang, Y. Shuai, and Y. Yu, "Fusion of satellite land surface albedo products across scales using a multiresolution tree method in the north central United States," *IEEE Trans. Geosci. Remote Sens.,* 2014, doi: 10.1109/tgrs.2013.2272935.

[7] *Advanced Remote Sensing: Terrestrial Information Extraction and Application*, S. Liang, X. Li, and J. Wang, Eds. Boston: Academic Press, 2012.

[8] C. B. Schaaf, F. Gao, A. H. Strahler, W. Lucht, X. W. Li, T. Tsang *et al.*, "First operational BRDF, albedo nadir reflectance products from MODIS," *Remote Sens. Environ.*, vol. 83, pp. 135–148, Nov. 2002.

[9] X. Y. Huang, Z. T. Jiao, Y. D. Dong, H. Zhang, and X. W. Li, "Analysis of BRDF and Albedo Retrieved by Kernel-Driven Models Using Field Measurements," *IEEE J. Sel. Top. Appl. Earth Observ. Remote Sens.*, vol. 6, no. 1, pp. 149–161, Feb. 2013.

[10] T. He, S. Liang, D. Wang, H. Wu, Y. Yu, and J. Wang, "Estimation of surface albedo and directional reflectance from Moderate Resolution Imaging Spectroradiometer (MODIS) observations," *Remote Sens. Environ.*, vol. 119, pp. 286–300, Apr. 2012.

[11] S. L. Liang, A. H. Strahler, and C. Walthall, "Retrieval of land surface albedo from satellite observations: A simulation study," *J. Appl. Meteorol.*, vol. 38, pp. 712–725, Jun. 1999.

[12] S. L. Liang, "A direct algorithm for estimating land surface broadband albedos from MODIS imagery," *IEEE Trans. Geosci. Remote Sens.*, vol. 41, no. 1, pp. 136–145, Jan. 2003.

[13] S. L. Liang, J. Stroeve, and J. E. Box, "Mapping daily snow/ice shortwave broadband albedo from Moderate Resolution Imaging Spectroradiometer (MODIS): The improved direct retrieval algorithm and validation with Greenland in situ measurement," *J. Geophys. Res.-Atmos.*, vol. 110, p. D10109, May 2005.

[14] D. Wang, S. Liang, T. He, and Y. Yu, "Direct estimation of land surface albedo from VIIRS data: algorithm improvement and preliminary validation," *J. Geophys. Res. Atmos.*, vol. 118, pp. 12,577–12,586, 2013.

[15] S. Liang, X. Zhao, S. Liu, W. Yuan, X. Cheng, Z. Xiao *et al.*, "A long-term Global LAnd Surface Satellite (GLASS) data-set for environmental studies," *Int. J. Digit. Earth*, vol. 6, pp. 5–33, 2013.

[16] Y. Qu, Q. Liu, S. Liang, L. Wang, N. Liu, and S. Liu, "Direct-estimation algorithm for mapping daily land-surface broadband albedo from MODIS data," *IEEE Trans. Geosci.Remote Sens.*, vol. 52, no. 2, pp. 907–919, Feb. 2014.

[17] T. H. Painter, J. Dozier, D. A. Roberts, R. E. Davis, and R. O. Green, "Retrieval of subpixel snow-covered area and grain size from imaging spectrometer data," *Remote Sens. Environ.*, vol. 85, pp. 64–77, Apr. 2003.

[18] S. L. Liang, "Narrowband to broadband conversions of land surface albedo I Algorithms," *Remote Sens. Environ.*, vol. 76, pp. 213–238, May 2001.

[19] S. L. Liang, C. J. Shuey, A. L. Russ, H. L. Fang, M. Z. Chen, C. L. Walthall *et al.*, "Narrowband to broadband conversions of land surface albedo: II. Validation," *Remote Sens. Environ.*, vol. 84, pp. 25–41, Jan. 2003.

[20] R. N. Clark, G. A. Swayze, R. Wise, E. Livo, T. Hoefen, R. Kokaly *et al.*, "USGS digital spectral library splib06a," *U.S. Geological Survey, Digital Data Series 231,* 2007.

[21] A. M. Baldridge, S. J. Hook, C. I. Grove, and G. Rivera, "The ASTER spectral library version 2.0," *Remote Sens. Environ.*, vol. 113, pp. 711–715, Apr. 2009.

[22] A. Berk, G. P. Anderson, P. K. Acharya, L. S. Bernstein, L. Muratov, J. Lee *et al.*, "MODTRAN5: 2006 update," in *Proc. SPIE 6233, Algorithms and Technol. Multispectral, Hyperspectral, Ultraspectral Imagery XII,* 2006, pp. 62331 F–62331 F-8.

[23] R. O. Green, M. L. Eastwood, C. M. Sarture, T. G. Chrien, M. Aronsson, B. J. Chippendale *et al.*, "Imaging spectroscopy and the Airborne Visible Infrared Imaging Spectrometer (AVIRIS)," *Remote Sens. Environ.*, vol. 65, pp. 227–248, Sep. 1998.

[24] S. Jacquemoud, W. Verhoef, F. Baret, C. Bacour, P. J. Zarco-Tejada, G. P. Asner *et al.*, "PROSPECT plus SAIL models: A review of use for vegetation characterization," *Remote Sens. Environ.*, vol. 113, pp. S56–S66, Sep. 2009.

[25] W. Verhoef, "Light-scattering by leaf layers with application to canopy reflectance modeling—the SAIL model," *Remote Sens. Environ.*, vol. 16, pp. 125–141, 1984.

[26] B. C. Gao, A. F. H. Goetz, and W. J. Wiscombe, "Cirrus cloud detection from airborne imaging spectrometer data using the 1.38 mu-m water-vapor band," *Geophys. Res. Lett.*, vol. 20, pp. 301–304, Feb. 1993.

[27] B. C. Gao and Y. J. Kaufman, "Water vapor retrievals using moderate resolution Imaging spectroradiometer (MODIS) near-infrared channels," *J. Geophys. Res. Atmos.*, vol. 108, p. 4389, Jul. 2003.

[28] Y. M. Shuai, J. G. Masek, F. Gao, and C. B. Schaaf, "An algorithm for the retrieval of 30-m snow-free albedo from Landsat surface reflectance and MODIS BRDF," *Remote Sens. Environ.*, vol. 115, pp. 2204–2216, Sep. 2011.

[29] J. G. Masek, C. Q. Huang, R. Wolfe, W. Cohen, F. Hall, J. Kutler *et al.*, "North American forest disturbance mapped from a decadal Landsat record," *Remote Sens. Environ.*, vol. 112, pp. 2914–2926, Jun. 2008.

[30] M. O. Roman, C. K. Gatebe, Y. Shuai, Z. Wang, F. Gao, J. G. Masek *et al.*, "Use of in situ and airborne multiangle data to assess MODIS- and Landsat-based estimates of directional reflectance and albedo," *IEEE Trans. Geosci. Remote Sens.*, vol. 51, no. 3, pp. 1393–1404, Mar. 2013.

[31] Y. M. Govaerts, B. Pinty, M. Taberner, and A. Lattanzio, "Spectral conversion of surface albedo derived from meteosat first generation observations," *IEEE Geosci. Remote Sens. Lett.*, vol. 3, no. 1, pp. 23–27, Jan. 2006.

Tao He received the B.E. degree in photogrammetry and remote sensing from Wuhan University, Wuhan, China, and Ph.D. degree in geography from the University of Maryland, College Park, MD, USA, in 2006 and 2012, respectively.

He has been a Research Associate with the Department of Geographical Sciences, University of Maryland. His areas of interest include surface anisotropy and albedo modeling, data fusion of satellite products, and long-term regional and global surface radiation budget analysis.

Shunlin Liang (M'94–F'13) received the M.S. degree in remote sensing and geographic information system in Nanjing University, China, in 1986. He received the Ph.D degree in geography from Boston University, Boston, MA, USA, in 1993.

Currently, he is a Professor with the Department of Geographical Sciences, University of Maryland, College Park, MD, USA, and the College of Global Change and Earth System Sciences, Beijing Normal University, Beijing, China. His main research interests focus on estimation of land surface variables from satellite data, earth energy balance, and assessment of environmental impacts of vegetation changes. He published about 180 peer-reviewed journal papers, authored the book "Quantitative Remote Sensing of Land Surfaces" (Wiley, 2004), edited the book "Advances in Land Remote Sensing: System, Modeling, Inversion and Application" (Springer, 2008), and co-edited the books "Advanced Remote Sensing: Terrestrial Information Extraction and Applications" (Academic Press, 2012), and "Land Surface Observation, Modeling, Data Assimilation" (World Scientific, 2013).

Dr. Liang is an Associate Editor of the IEEE Transaction on Geoscience and Remote Sensing and also a guest editor of several remote sensing related journals.

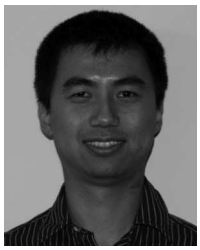

Dongdong Wang received his B.S. and M.Sc from Peking University, China in 2002 and 2005 respectively. He received the Ph.D. degree from the University of Maryland, College Park in 2009.

Currently, he is a Research Assistant Professor with the Department of Geographical Sciences, University of Maryland. His primary research interests include retrieval of biophysical and flux parameters and spatio-temporal analysis of these variables.

Qinqing Shi received the B.S. degree in electronics engineering and computer science from Peking University, Beijing, China in 2011. She is currently working toward the Ph.D. degree at the Department of Geography, University of Maryland, College Park, MD, USA.

She is a Graduate Research Assistant with the Department of Geography, University of Maryland. Her research interests include analysis of the surface energy budgets over the Tibetan Plateau and its relationship to the Asian summer monsoon.

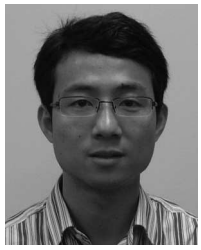

Xin Tao received the B.S and M.E. degrees from Peking University, Beijing, China, in 2006 and 2009, respectively. He is currently working toward the Ph.D. degree at the Department of Geographical Sciences at University of Maryland, College Park, MD, USA.

His research interests are focused on estimation of biogeophysical variables from satellite data and data fusion of satellite products.